# Preliminary mapping of liquefaction phenomena triggered by the February 6 2023 M7.7 earthquake, Türkiye / Syria, based on remote sensing data

M. Taftsoglou, S. Valkaniotis, E. Karantanellis,

E. Goula, G. Papathanassiou

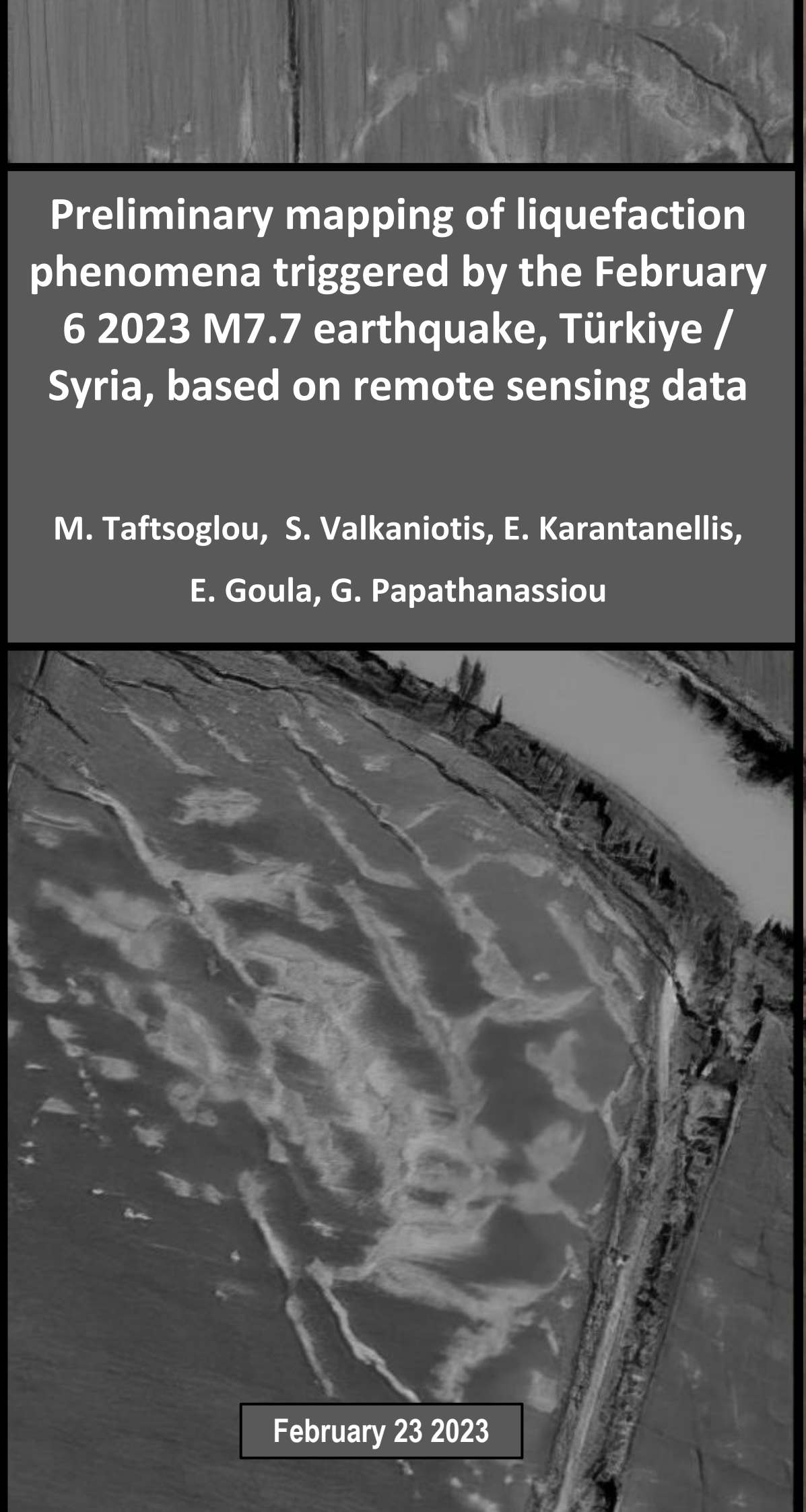

February 23 2023

# Preliminary mapping of liquefaction phenomena triggered by the February 6 2023 M7.7 earthquake, Türkiye / Syria, based on remote sensing data

**Taftsoglou M. [1], Valkaniotis S. [1], Karantanellis E.[2], Goula E.[3], Papathanassiou G. [3]**

1. Department of Civil Engineering, Democritus University of Thrace, Greece

mtaftsog@civil.duth.gr

svalkani@civil.duth.gr

2. Department of Earth and Environmental Sciences, University of Michigan, USA

stratis@umich.edu

3. Department of Geology, Aristotle University of Thessaloniki, Greece

gevmorfi@geo.auth.gr

gpapatha@geo.auth.gr

**The report is available in the Zenodo repository: https://doi.org/10.5281/zenodo.7668401**

## 1. Overview of the events

On the 6th of February 2023, a strong earthquake doublet of Mw 7.7 and Mw 7.6 (AFAD) respectively occurred in SE Türkiye and northern Syria. The earthquakes hit the provinces of Kahramanmaraş, Adıyaman, Hatay, Osmaniye, Gaziantep, Kilis, Şanlıurfa, Diyarbakır, Malatya, Adana, and Elazığ. The first event of Nurdağı-Pazarcık Earthquake nucleated ~15km of the mapped trace of the East Anatolian Fault Zone (EAFZ) and approximately 40 km north-west of Gaziantep, and 33 km south-east of Kahramanmaraş, with a focal depth of 8.6 km (AFAD). The spatial distribution of aftershocks indicates that the earthquake rupture reached Antakya (Hatay) in the south and come to an end in the north at the Pütürge segment close to the Doğanyol, Elazığ earthquake in 2020 (Melgar et al. 2020, Taymaz et al. 2021).

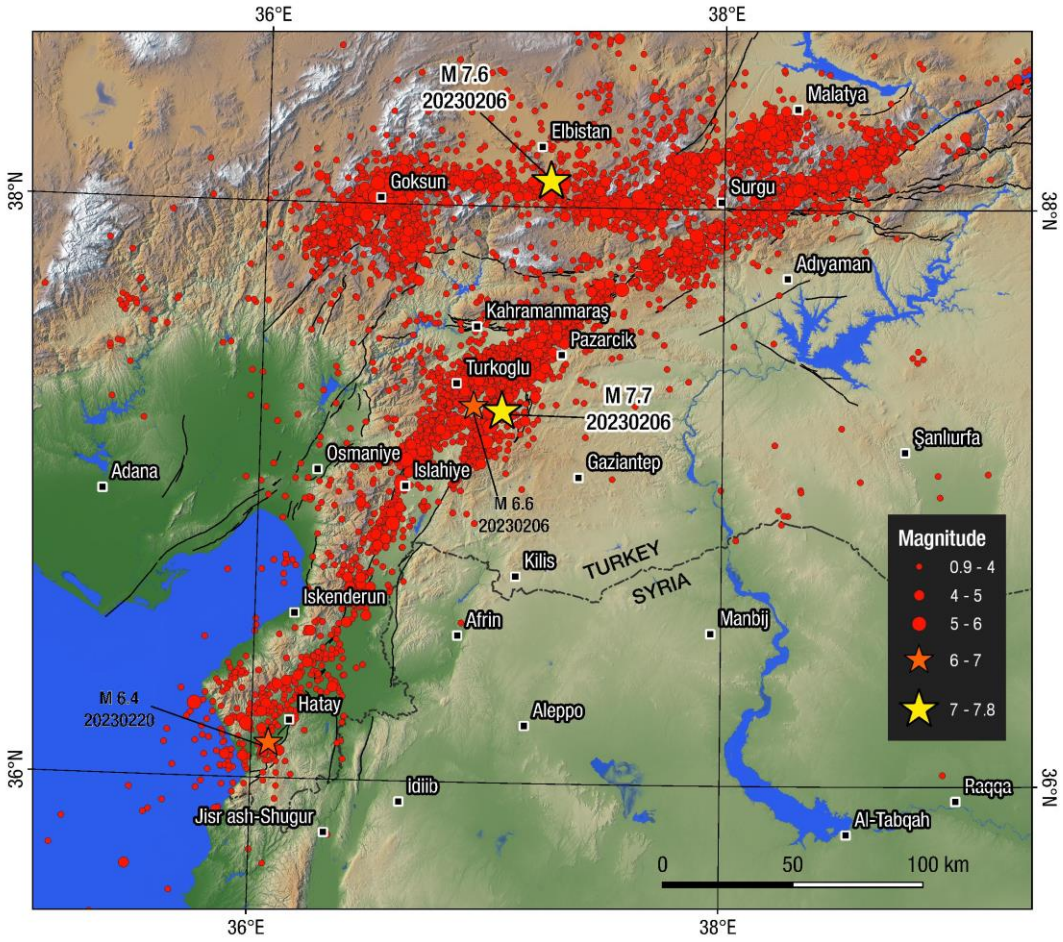


**Figure 1.** Overview of aftershocks for the M7.7 and M7.6 earthquakes. Extent of aftershocks mark the ruptured fault segments. Epicenter locations from AFAD catalogue (06/2/2023 – 21/2/2023).

Nine hours after Nurdağı-Pazarcık Earthquake the second event took place at Ekinözü, closed to the mapped trace of the Sürgü fault, and approximately 98 km north-west of Adıyaman, and 62 km north-east of Kahramanmaraş, with a focal depth of 7.0 km (AFAD). Seismic data indicate that the earthquake initially ruptured the ~E-W trending Çardak fault which strike more southwards in the west and continued eastward towards Malatya on the NE-SW trending Doğanşehir fault zone. Ekinözü earthquake is considered as a part of "doublet" rather than a mainshock/aftershock sequence, because is located on a separate structure with large magnitude value (Taymaz et al. 2022). Analyses of teleseismic data for

both cases revealed almost pure left-lateral strike-slip motion on a nearly vertical NE-SW trending fault (Melgar et al. 2023).

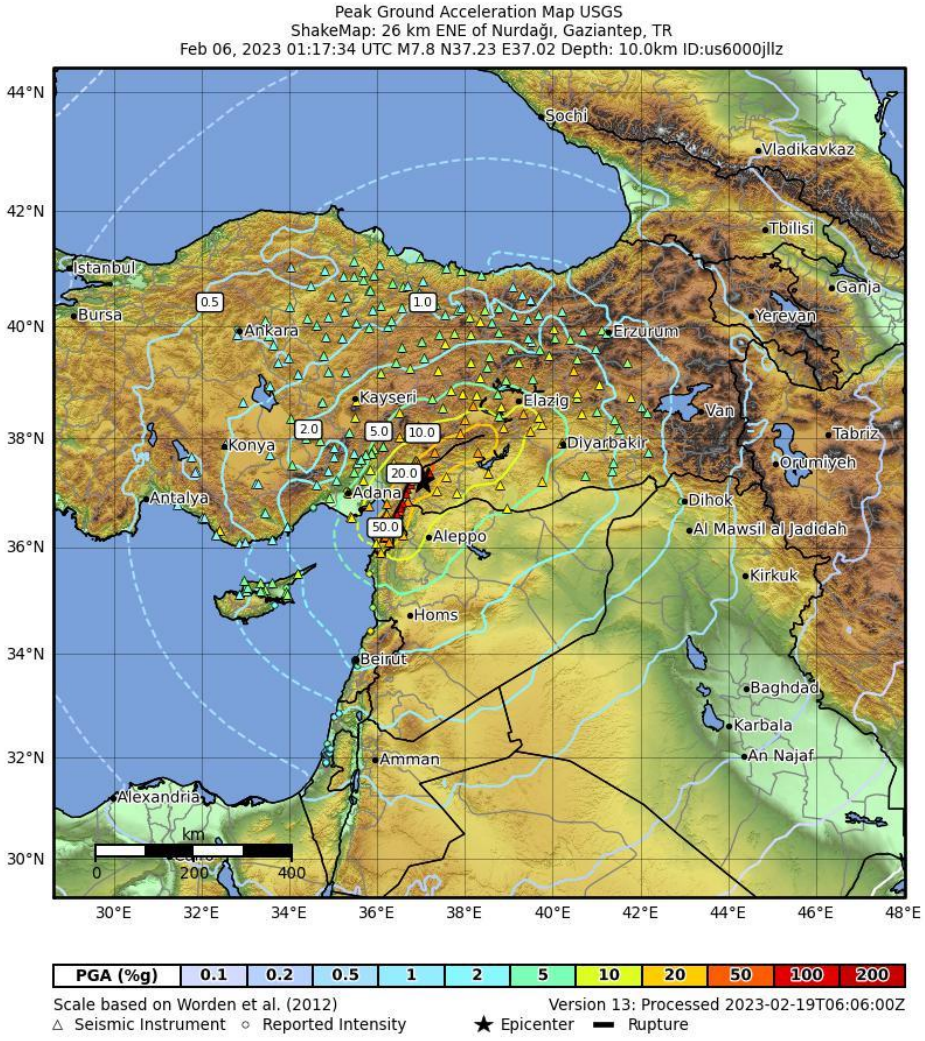


**Figure 2.** Peak Ground Acceleration map, from the USGS ShakeMap for the M7.7 earthquake.

## 2. Regional Tectonics and geological setting of EAFZ

The East Anatolian Fault Zone (EAFZ) forms a 580-km long plate boundary between the Arabian and Anatolian microplates (Allen 1969; Duman & Emre 2013) and is associated with frequent shallow seismicity in the top ~20-25 km of the crust and strike-slip type tectonism (Taymaz et al., 1991; Tan and Taymaz, 2006; Melgar et al. 2020a; Taymaz et al. 2021). It consists of several minor, but two major active strands; southern strand spanning from Karliova to Antakya linking the Dead Sea Fault Zone (DSFZ) and the Cyprus Arc around the Amik triple junction (~580 km long) and northern strand due to partitioning around the town of Çelikhan towards the Sürgü-Kozan-Misis fault system, which is ~350 km long and merges with the Misis fault zone in the Gulf of Iskenderun

In eastern Turkey and northwest Syria, the relative plate motion is accommodated by left lateral strike slip faulting at slip rates 10±1 mm/yr (Reilinger et al., 2006). Furthermore, latest research of EAFZ fault's activity indicates the displacement of Euphrates River by 12 km since the mid-Quaternary (Trifonov et al. 2018) thus attaining a mean geological slip rate

of 12-15 mm/yr. This dynamic motion has initiated large number of destructive earthquakes, in the last 2000 years. Previous large events along the EAFZ include 1964 Malatya Ms 5.7, 1971 Bingol Ms 6.9, 1986 Dogansehir-Malatya Ms 5.9, 2003 Bingol Mw 6.3, 2004 Sivrice Mw 5.5, 2010 Kovancılar-Elazıg Mw 6.1 earthquakes and 2020 Doganyol-Sivrice Mw 6.7 . Other major earthquakes include the 1975 Lice Ms 6.7 and 1992 Erzincan Mw 6.7 events which were accompanied by many significant aftershocks on the highly stressed segments of nearby North Anatolian Fault Zone and Southeast Anatolian Thrust Zone.

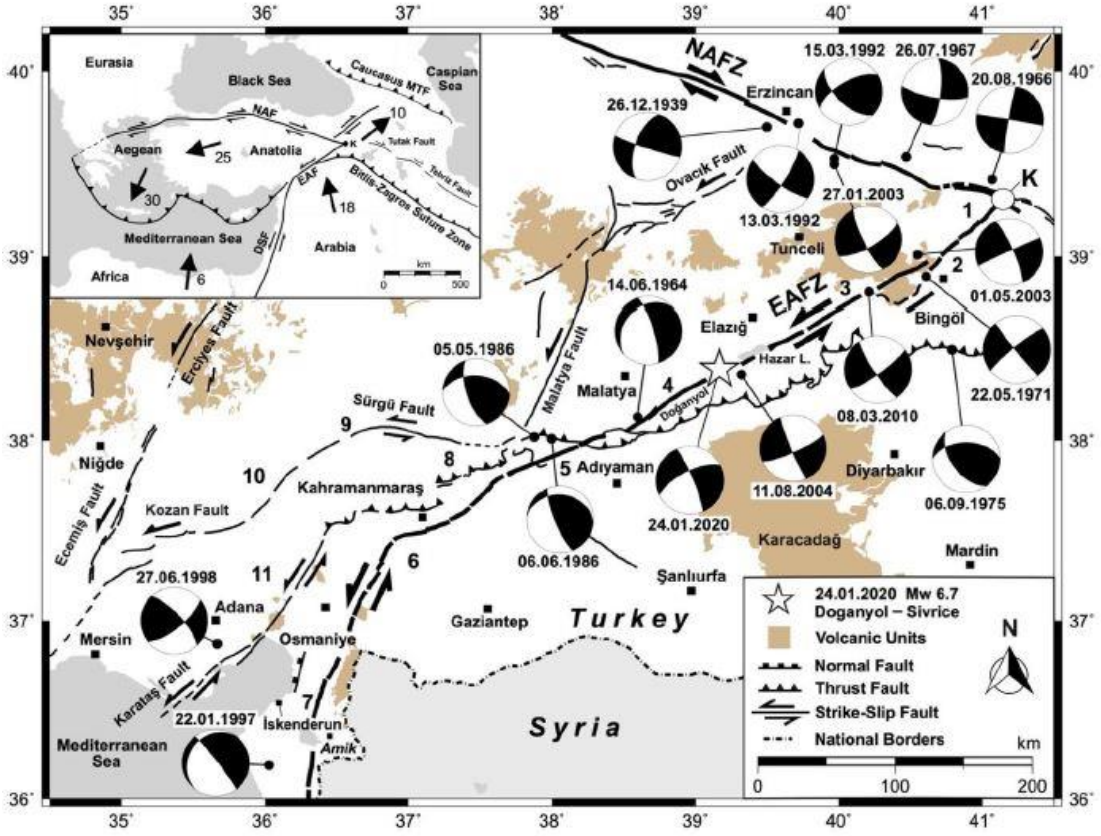


**Figure 3.** Summary and location map (from Taymaz et al. 2021) of the East Anatolian Fault Zone (EAFZ) composed by interpretations and observations of Şaroğlu et al. (1992a, 1992b) and Duman and Emre (2013). 1: Karlıova segment; 2: Ilıca segment; 3: Gökdere restraining segment; 4: Palu segment; 5: Pütürge segment; 6: Ekenek segment; 7: Pazarcık segment; 8: Sürgü fault segment; 9: Çardak fault segment and Göksun releasing stepover; 10: Savrun fault zone and 11: Karataş releasing bend along with major volcanic fields (e.g. Karacadağ). Inset box at the upper-left displays the regional tectonic setting, comprising relative motions of the Arabian and African plates, central Turkey and the southern Aegean Sea relative to Eurasia modified after Taymaz et al. (1991b), Tan and Taymaz (2006), Yolsal-Çevikbilen et al. (2012, 2014) and references therein. The black arrows with numbers indicate direction of tectonic motion relative to Eurasia and velocity (mm/yr) obtained from GPS data (McClusky et al. 2000). DSF: Dead Sea Fault; EAFZ: East Anatolian Fault Zone, K: Karliova Triple Junction; MTF: Main Thrust Zone; NAFZ: North Anatolian Fault Zone.

The EAF cuts through mountainous terrain with elevations ranging between 1–2 km forming complicated structures with continuous, linear valleys where several pull-apart basins, conjugate fractures and moreover considerable thrusting and folding are visible on the landscape of its hinterland exposing the major active fault segments and fractures mapped in the region, as well as in the Arabian foreland. The local geology includes Palaeozoic–Mesozoic metamorphic rocks, Mesozoic ophiolitic mélange and volcanic rocks (Hempton 1985) that have deformed during the Early-Tertiary closure of Neotethys ocean and the

south-directed obduction of ophiolites towards the Arabian foreland (Şaroğlu et al., 1992a, 1992b; Herece 2008; Duman and Emre, 2013). Within EAF and DSFZ is located the transition zone of the Karasu Rift, characterized by active faulting, basaltic volcanism and sedimentation during Quaternary. Surrounded by Amanos Mountains to the west and Kurt Mountains to the east, the valley is filled with fluvial and lacustrine sediments interfingered and covered with the volcanic sequence. To the southwest Karasu rift connects with Amik Basin, located in the junction of Asi Valley in south and Antakya-Samandag Corridor in southeast.

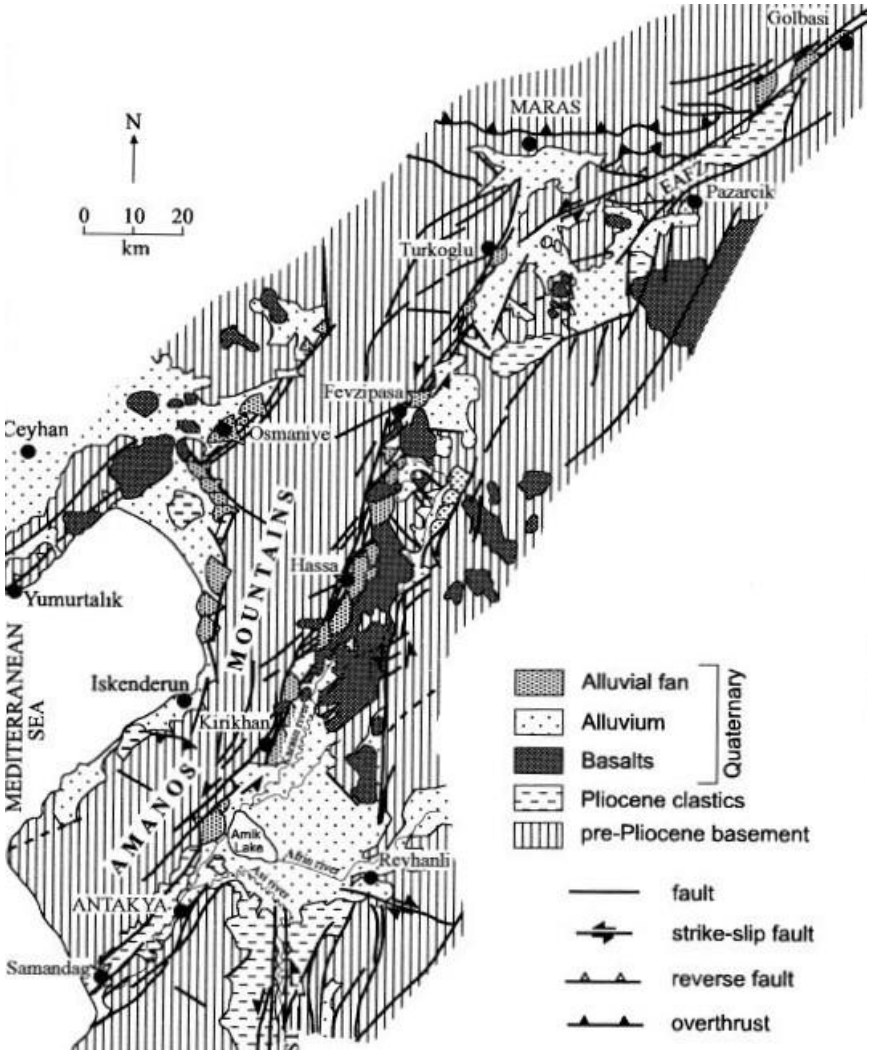


**Figure 4.** Regional geological map of the Karasu Rift. (simplified from 1:500000 by Rojay et al.2001) DST: Dead Sea transform fault zone, EAFZ: East Anatolian fault zone.

### 3. Historical seismicity at the Hatay, Antakya basin

The area of Antakya is located at the southeastern part of Turkey, near the intersection of several regional-scale structural lineaments of Cenozoic age, namely the Dead Sea Fault Zone, the East Anatolian Fault Zone and the Cyprus Arc. Seeking in the literature, more than twenty (20) earthquakes occurred the last 20 centuries that heavily damaged the cities within this area. The earthquake-induced failures were reported, documented, and presented in seismic catalogues such as Ambraseys N. & Finkel C.F. 1995, Ambraseys N. 2009, Guidiboni Em. & Comastri Al., 1994 and 2005. In this preliminary report, we focused

on the events that triggered liquefaction-related phenomena, which are briefly presented below.

Taking into account the information provided by these catalogues, it is concluded at least 4 earthquakes triggered secondary effects that are likely to be related to the liquefaction of subsoil layers. The oldest case is related to an earthquake occurred in Antioch on 14 September 458 AD causing several destructions of the buildings, many deaths and injuries. The event resulted to ground opening in places probably due to slumping of the soft river deposits on which the new part of the city had been built (Ambraseys 2009). On 29 March 526 AD, a serious earthquake in the region of Antioch caused the death of 250.000 people, the devastation of the city and surrounding areas and the distraction of the port of Seleucia Pieria. Aftershocks continued for six months, presumably causing additional damage. According to the literature, both the city of Antioch and half of the city of Pompeiopolis were swallowed up. In addition, in the lower part of the city of Antioch, a mixture of water and sand was ejected from the ground and buildings sank into their foundations (Ambraseys 2009). The earthquake occurred on 29 November 1114, was so severe that almost caused the complete destruction of Antioch. In the suburbs of Antioch the earth opened up while many towers and houses were swallowed up. In addition, the city of Sanosata (Sumaisat), built on the left bank of the Euphrates, was heavily damaged; houses collapsed in some parts of the town and elsewhere sank into their foundations. (Guidoboni & Comastri 2005; Ambraseys 2009).

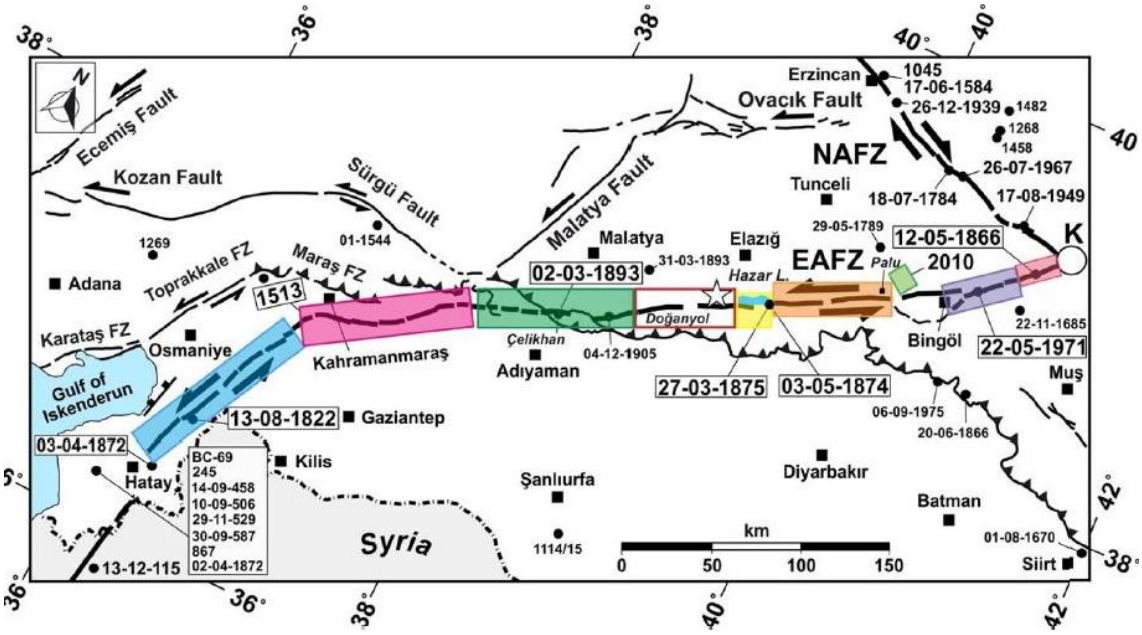


**Figure 5.** Surface breaks of the active fault segments highlighted in colours produced by large earthquakes along the EAFZ (Ambraseys 1989; Ambraseys and Jackson, 1998; Duman & Emre, 2013). February 06 2023 M7.7 earthquake ruptured through the 1822, 1513 and 1893 ruptured segments. The rectangle box outlined in red-lines spots the locked fault "seismic-gap" filled by the 24 January 2020 $M_w$ 6.7 Doğanyol-Sivrice earthquake (white star). EAFZ: East Anatolian Fault Zone; NAFZ: North Anatolian Fault Zone. Large white circle marked with K spots the location of Karliova triple junction. Figure from Taymaz et al. 2021.

Finally, on 13 August 1822 a large earthquake occurred in Southeastern Anatolia. The shock almost destroyed the region between Gaziantep and Antakya in Turkey and Aleppo and Han Sheikhun in northwestern Syria, killing a large number of people. The ground opened up at

the Orontes River and overflowed its banks, while the destruction of the embankments resulted to the flooding of cultivated lands. Water issued from many of the crevasses induced by the earthquake in the low ground near the city of Antakya and in the Amik valley. Finally, some houses near the old port at Payas sank into the ground (Ambraseys 2009).

## 4. Rapid mapping of liquefaction phenomena

After the devastating M7.7 and M7.6 earthquakes struck, we collected all available satellite and remote sensing data over the affected area, as soon as they became available. We encountered difficulties concerning cloud cover and snow cover over the area, especially the northern part where most of the areas of interest are still covered by recent snowfall.

Based on methodology previously applied in earthquake events (Hauksson et al. 2020, Papathanassiou et al. 2022) we used optical satellite imagery from Copernicus Sentinel-2 multispectral sensor, with a ground resolution of 10m, to scan for indications of significant liquefaction features. The first Sentinel-2 acquisitions over the area took place in February 9, three days after the strong earthquakes. Our search was focused on candidate areas that have extended Holocene fluvial and lacustrine sediments, with flat relief and relatively close to the fault rupture, and wide fluvial valleys. Sentinel-2 imagery can identify large liquefaction features but it's not suitable for mapping individual features or manifestations. Following the identification of a number of candidate areas, we used very high resolution (VHR) optical satellite imagery provided by Maxar Open Data program (with a ground resolution of 0.3-0.7m). VHR data coverage was limited, thus we used Planet optical imagery (ground resolution 3m) to cover a wider search area. At a few locations, we utilized additional available source, such as response UAV orthophotos (OpenAerialMap) and Copernicus Emergency Mapping Service (EMS) imagery at key urban areas. Post-earthquake imagery was dated from February 06 up to February 12 2023. Copernicus Sentinel-1 SAR imagery was used for interferometric analysis and coherence mapping.

We have identified 760 sites with liquefaction and lateral spreading features, along a 250km section of the East Anatolian Fault Zone rupture (Figure 6). The northernmost area where we were able to identify liquefaction phenomena was Golbasi lake, at the NE part of the M7.7 earthquake rupture. Mapping at a higher latitude was limited by snow cover and limited availability of VHR imagery. From the extent of the mapped liquefaction phenomena, we consider those to be triggered by the first M7.7 rupture, early in Feb 06, and do not include liquefaction from the second M7.6 earthquake to the north.

Unexpectedly, most liquefaction and lateral spreading sites manifested along and near coastal sites, fluvial valleys and drained lake/swamp areas, covered by Holocene loose sediments. The following figure shows the distribution of mapped liquefaction sites along the fault rupture and shows that most concentrations are found in Holocene sediment-filled basins.

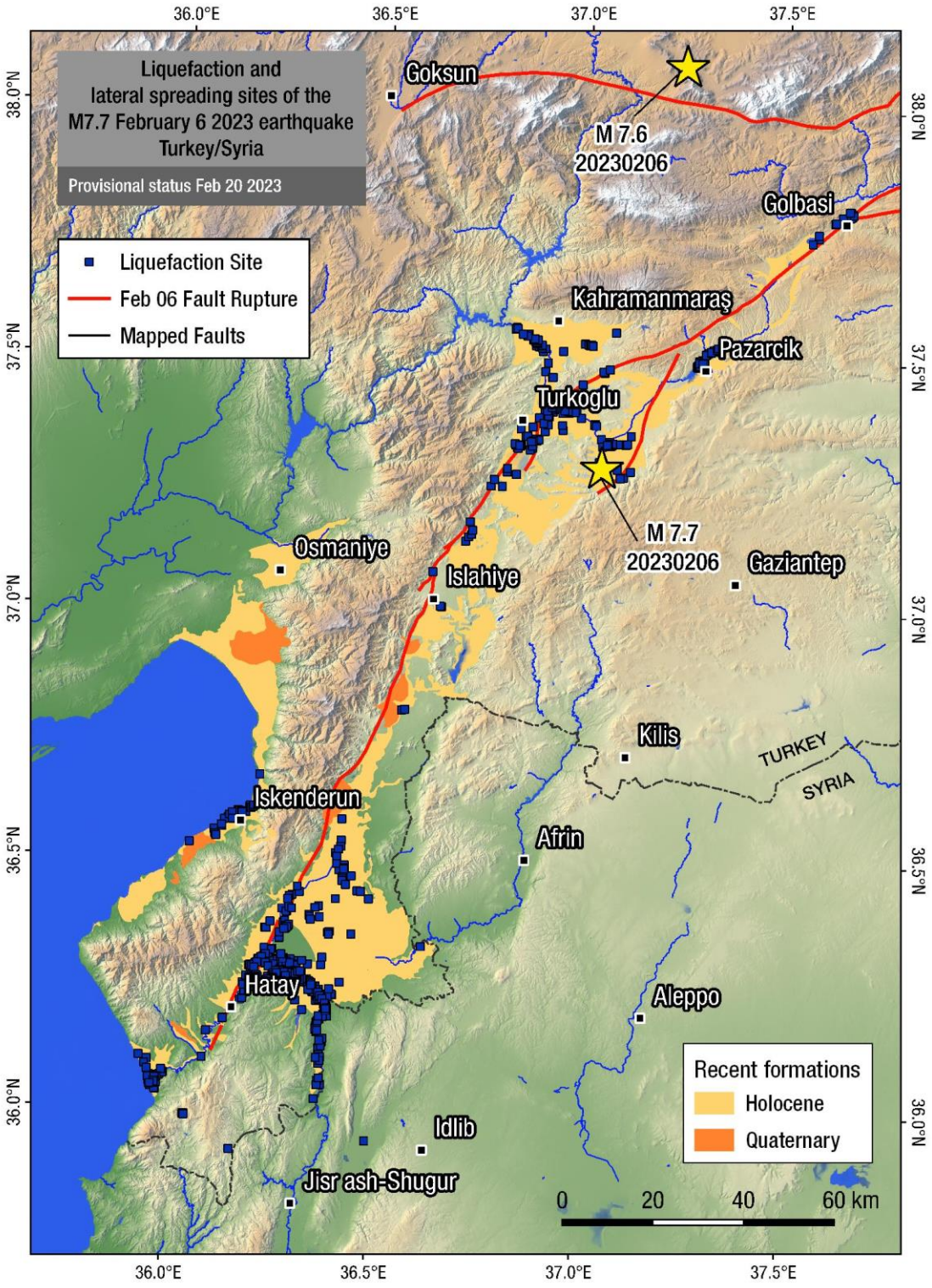


**Figure 6.** Overview map of liquefaction and lateral spreading sites identified and mapped using satellite imagery. Areas with major concentrations of liquefaction manifestations are Amik plain north of Hatay/Antakya, the extensive fluvial basins near to the M7.7 epicenter and the coastal plains of Hatay/Antakya and Iskenderun. Simplified geology from MTA (2002).

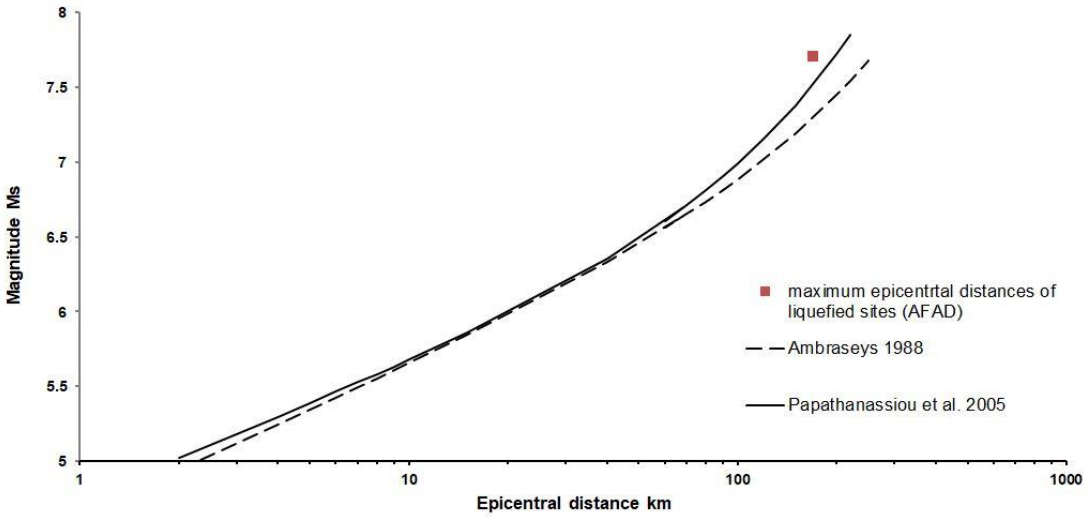


**Figure 7.** Maximum epicentral distance and comparison to the proposed curves for the assessment of liquefaction susceptibility (Ambraseys 1988, Papathanassiou et al. 2005 & Papathanassiou et al. 2016).

## 5. Key findings and locations

Most of the sites identified in remote sensing data are found along the main M7.7 fault rupture of the southern section of the Eastern Anatolian Fault Zone. Liquefaction manifestations are found from Antakya coastal plain up to Golbasi lake to the northeast. North of Golbasi and along the M7.6 Sürgü fault rupture snow cover and limited remote sensing data prohibit a remote mapping effort for the moment, until new imagery is acquired and weather conditions improve.

Apart from the sites depicted in Figure 6, there was a number of candidate sites mapped in areas further from the EAFZ, like Idlib and the coastal area north of Iskenderun. We excluded these sites upon further examination with higher resolution data.

The area most affected by liquefaction and lateral spreading is Amik plain and Orontes (Asi) river plain, north of Antakya (Figure 8). Amik (Amuq) plain is a transtensional sedimentary basin, formed in the meeting point of Eastern Anatolian Fault Zone and the Dead Sea Fault Zone (Coskun 1994, Yener et al. 2000, Karatas 2014). Amik plain is covered by Holocene fluviolacustrine sediments above a succession of Tertiary sediments with a thickness of 200-300 meters. The central-western part of the plain was covered by Amik lake, drained in the early 1970's. Three main rivers are exiting through Amik plain, Kara Su from the north, Afrin river from the east and Orontes (Asi) river from the south. Orontes river is exiting to the south through Antakya, while Afrin and Kara Su are being drained by an extensive canal system.

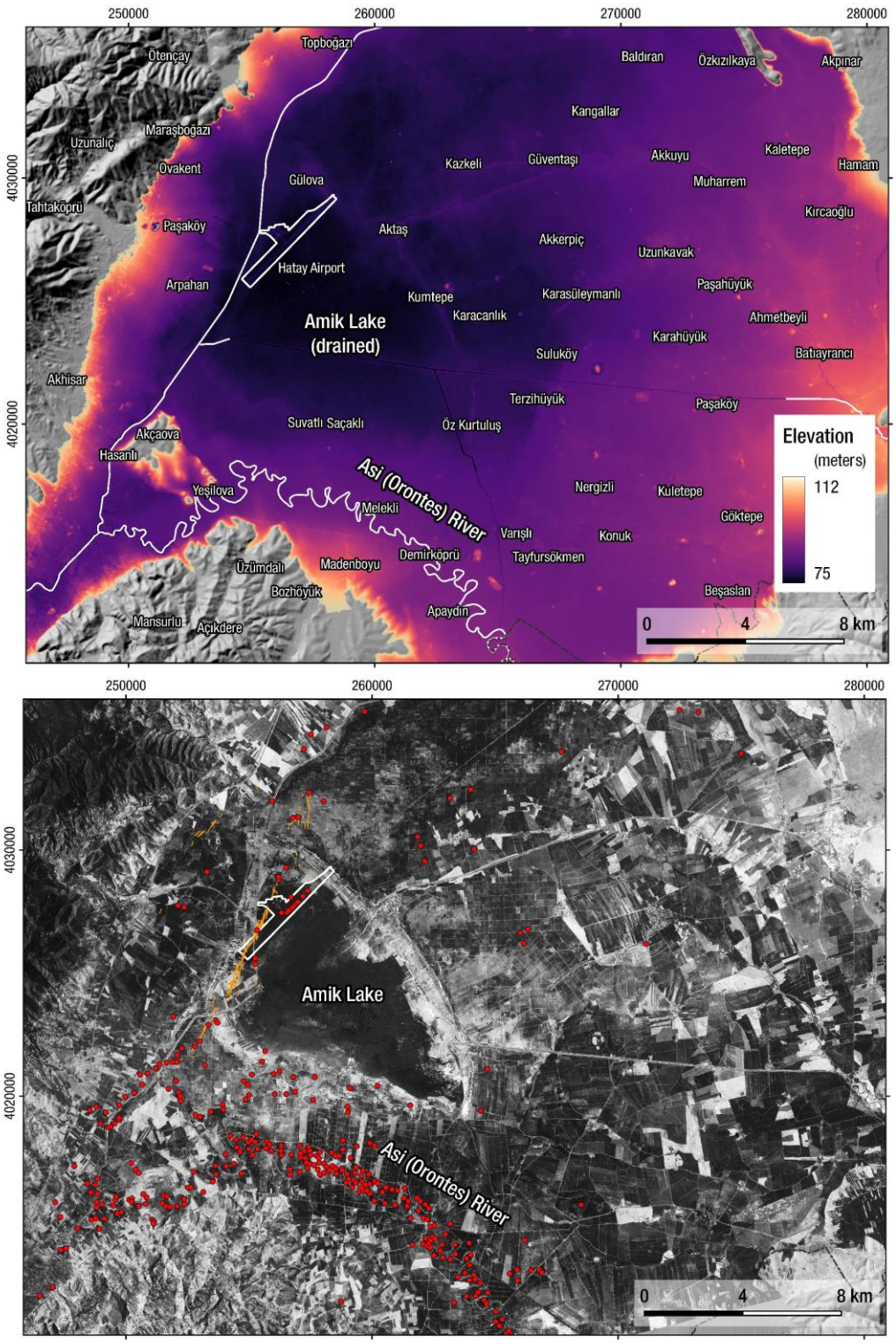


**Figure 8.** Above: Elevation map of Amik (Amuq) plain, north of Antakya. Low elevation areas (dark) mark the extent of the drained Amik lake. Hatay airport and the major canal to the west, with Asi (Orontes) river meander to the south. Elevation source: Copernicus DEM. Below: Corona declassified satellite imagery from 1969, showing the last extent of Amik lake. Liquefaction related phenomena are marked with red, and orange lines show the mapped earthquake surface ruptures and cracks through the Hatay airport.

The southernmost branch that ruptured during the M7.7 earthquake, is found along the western part of Amik basin, with extensive surface ruptures. Surface ruptures from this segment damaged the westernmost part of Hatay airport and the main water canal, leading to local flooding of large areas of the former lake. Reported damages on the airport runway are attributed not to faulting but deformation of the runway embankment/fill by liquefaction related phenomena. Liquefaction sites were mapped mostly in the surroundings of the former lake bed and along the meanders of Orontes river. Flooding of Orontes river along Asi valley up to the border of Turkey-Syria masked a large number of liquefaction phenomena. We managed to map a portion of the later-submerged area from an image acquired in February 06.

We used interferometric coherence from processing pre- and co-seismic pairs of Copernicus Sentinel-1 SAR imagery. Loss of coherence is an indication of possible widespread liquefaction and lateral spreading at a location. While interferometric pairs from the M7.7 earthquake had a number of difficulties, including masking of the signal by the wide deformation of the main fault ruptures, they provided a guide for identifying candidate locations (Fig.10).

A significant number of liquefaction and lateral spreading phenomena was also mapped in Iskenderun port city, Golbasi lake and the coastal plain of Samandag, where Orontes river is exiting through Antakya city.

Iskenderun (Alexandretta) port city was severely damaged due to widespread lateral spreading and liquefaction along it’s coastal front. Large areas were inundated and sections of piers were submerged due to lateral spreading (Fig.12).

Gölbası lake is formed within a series of pull-apart basin along the main strand of Eastern Anatolian Fault Zone. We mapped extensive lateral spreading deformation along the northern, eastern and southern coast of the lake, where a few areas were visibly submerged in post-earthquake imagery. Damaging liquefaction and lateral spreading occurred also within Gölbası town (Fig. 13 & 14).

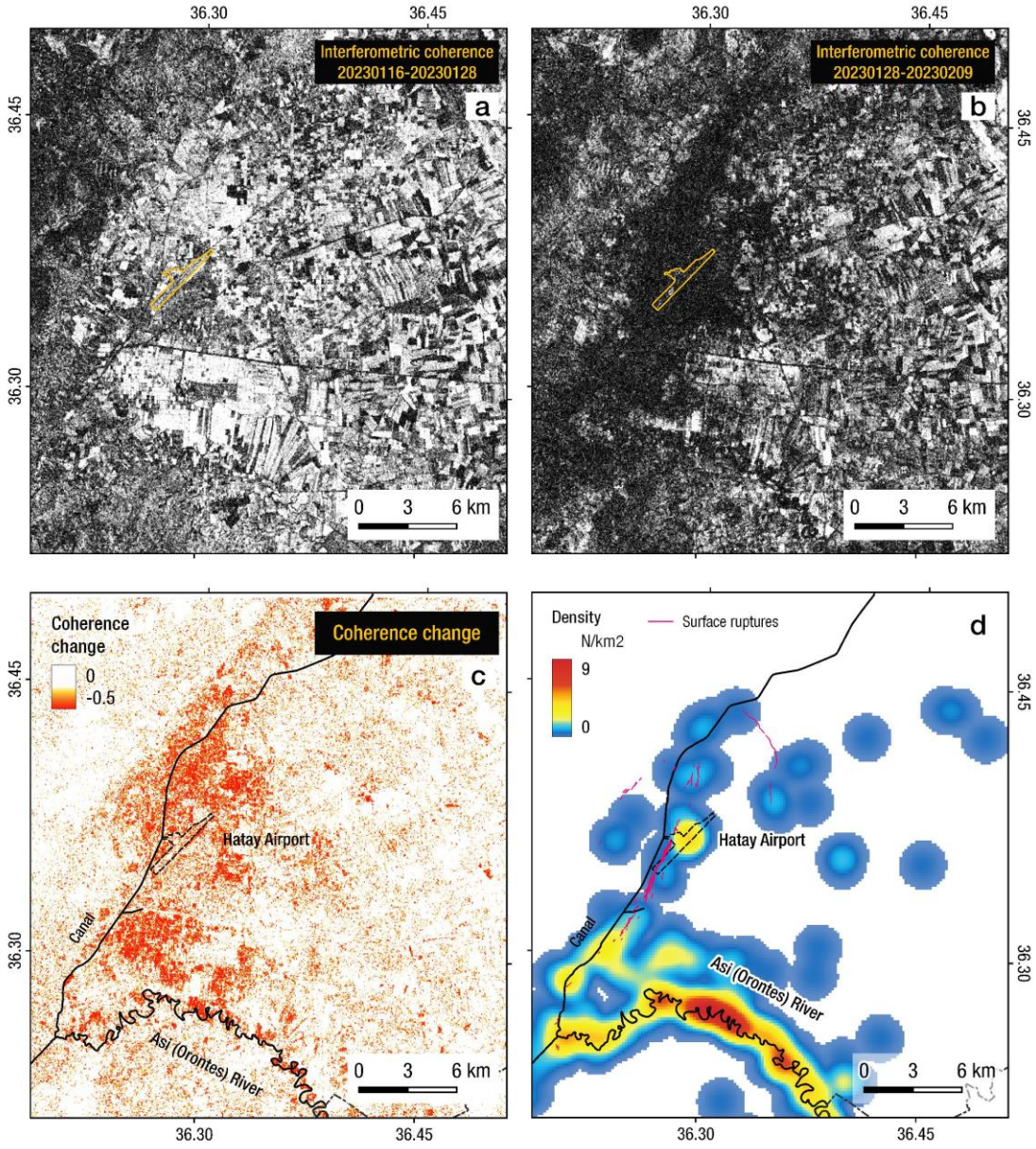


**Figure 9.** Interferometric coherence of Amik plain area from before the earthquake (a) and co-seismic interval (b). Darker colors correspond to coherence loss due to ground surface disturbance and land cover changes. Distribution of high values of coherence change between the two datasets (c) coincides with high density of mapped liquefaction features (d) to the south and south-west, flooded areas along the western canal, and also along the NNE-SSW axis of co-seismic ruptures west of the airport.

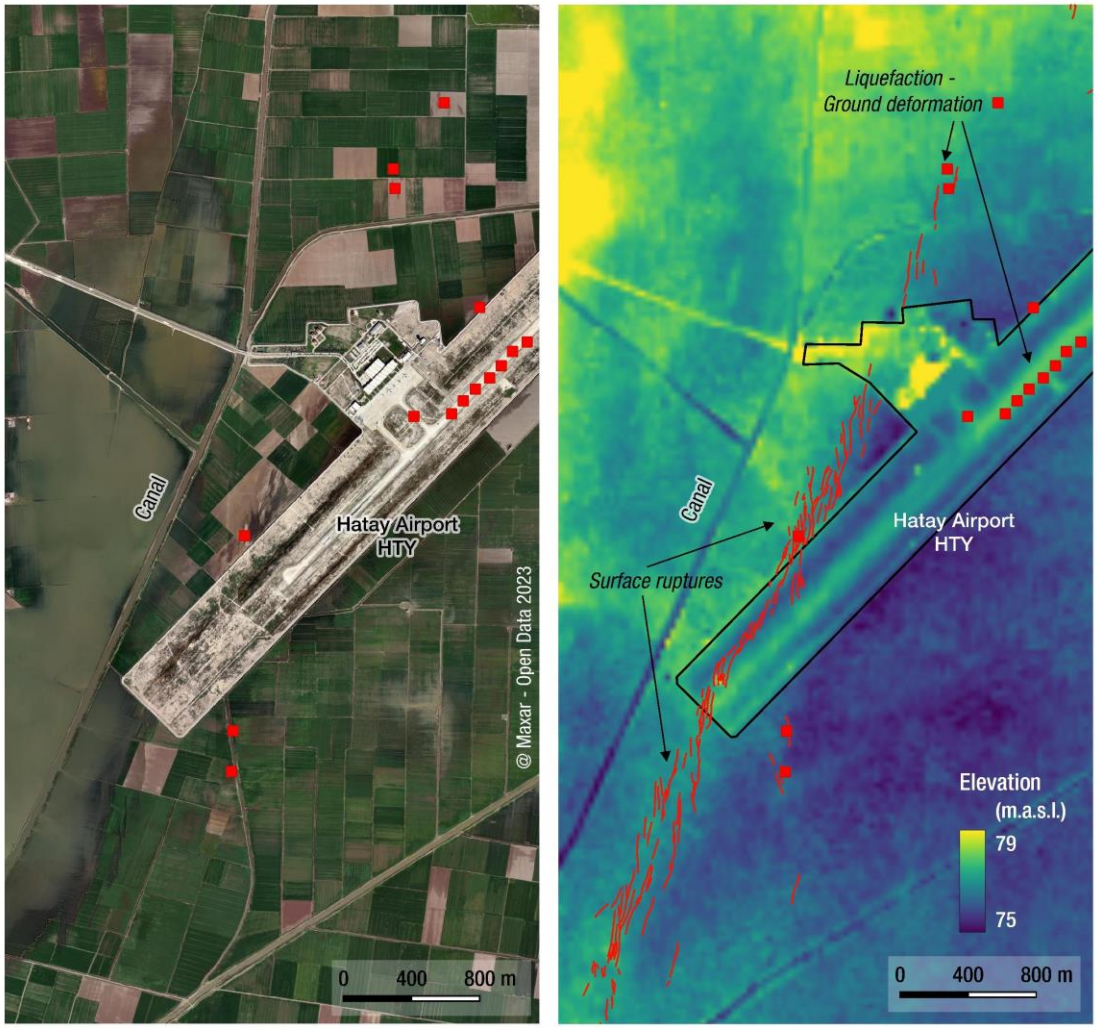


**Figure 10.** Left: post-earthquake satellite imagery of Hatay airport in Amik plain (Maxar Open Data program). Right: mapped surface ruptures and ground cracks (red lines) and liquefaction related phenomena (red symbols). Fault rupture crossed through the western area of the airport, but damage to the runways is attributed to liquefaction and failure of the runway fill. Elevation source: Copernicus DEM.

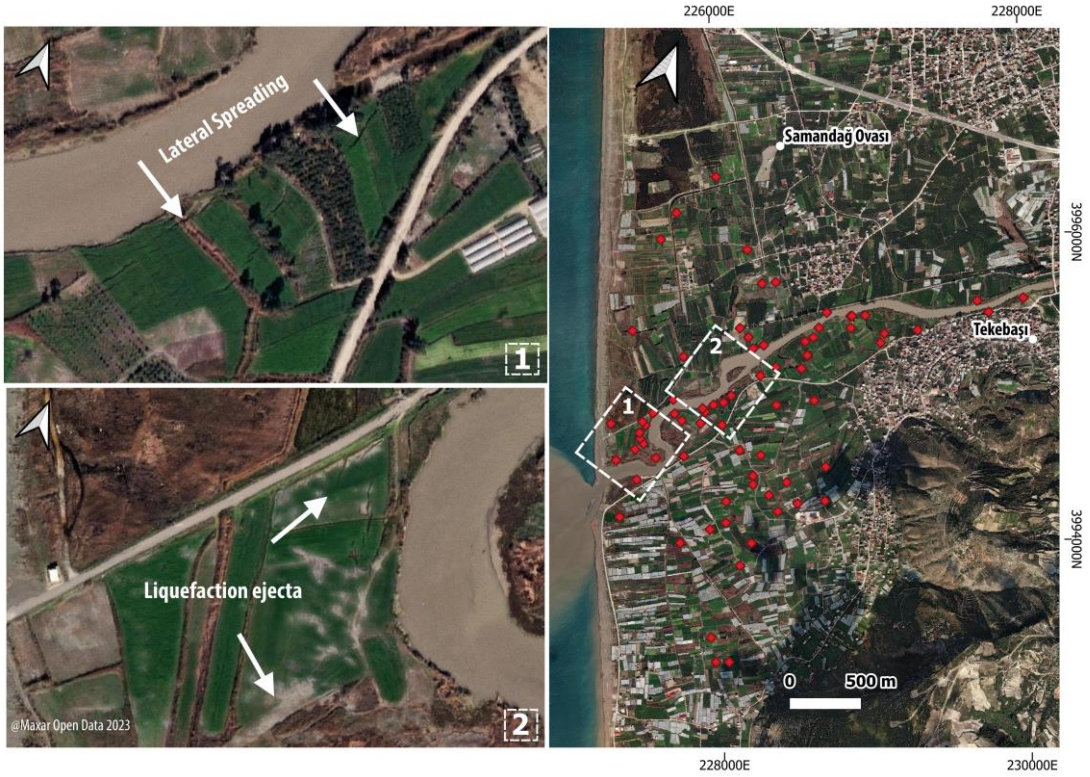


**Figure 11.** Liquefaction and lateral spreading sites at the coastal plain south of Antakya. Most of the sites are found along the course of Asi (Orontes) river and over abandoned fluvial features.

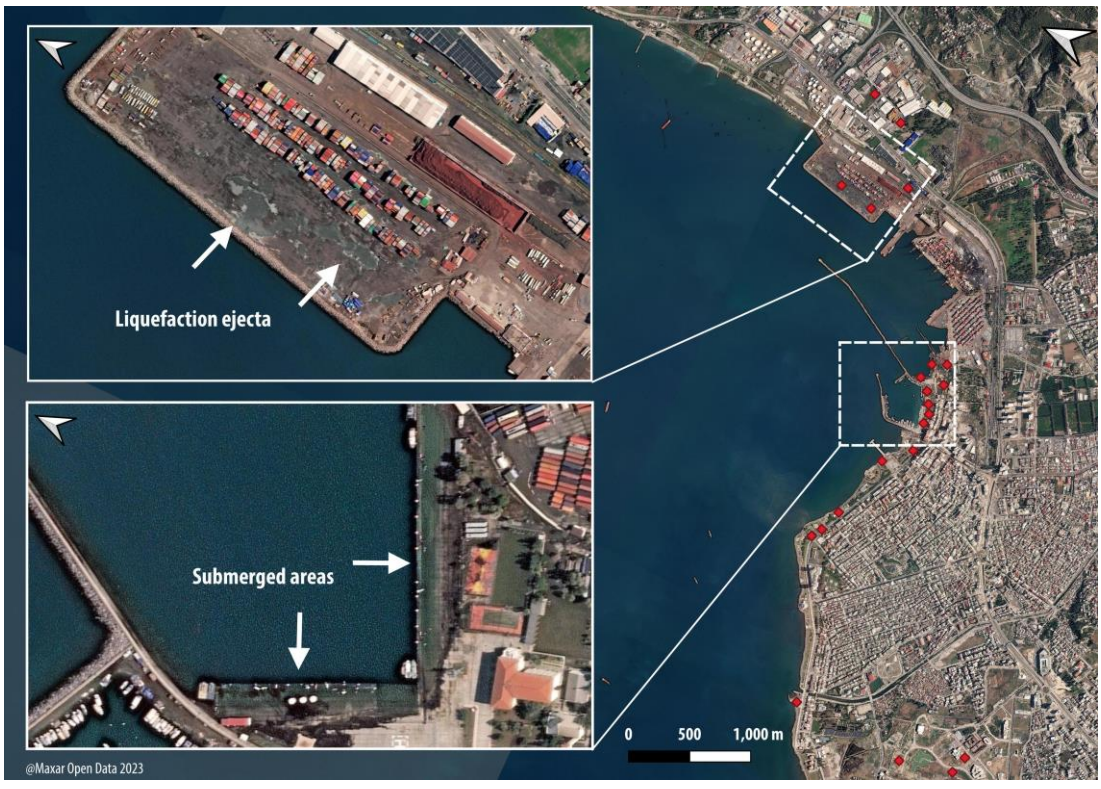


**Figure 12.** Liquefaction and lateral spreading sites at the port city of Iskenderun. Most of the sites were found along the coastal front and within the reclaimed port facilities and piers of the old port. Insets show liquefaction ejecta and submerged sections of piers. Widespread lateral spreading and subsidence was manifested along a > 6km section of the coastal front.

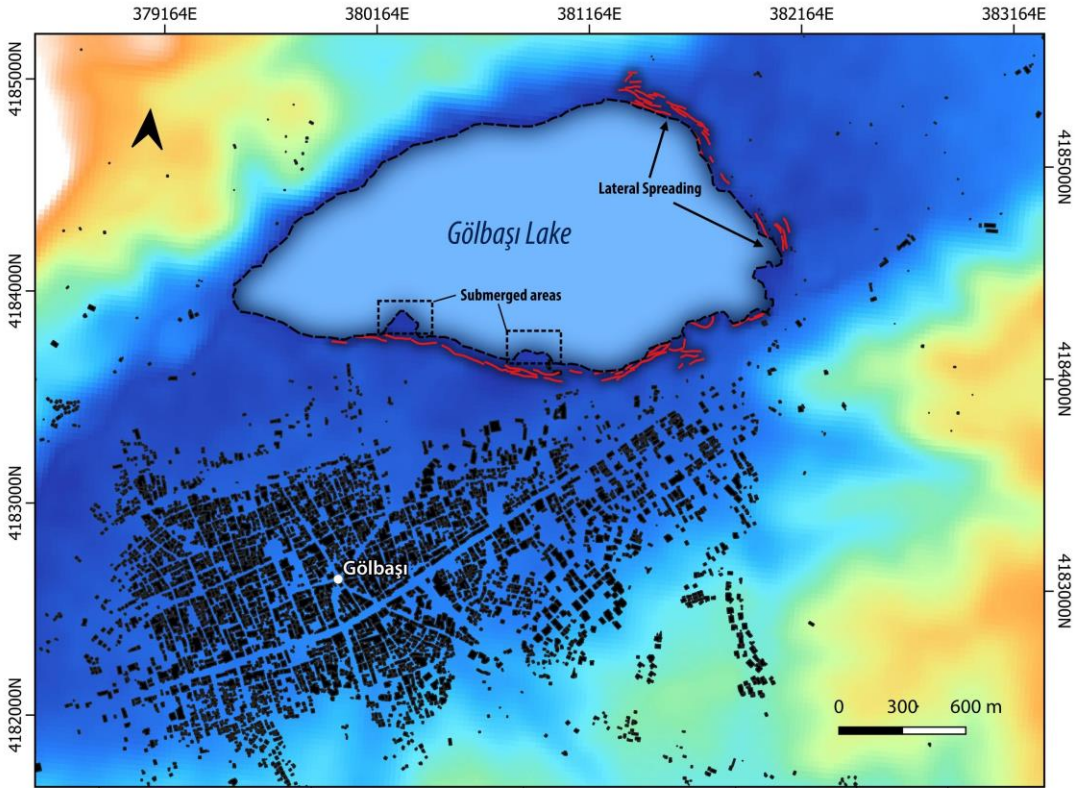


**Figure 13.** Widespread lateral spreading along the coastline of Gölbası lake (red lines). A small delta and parts of southern coast were submerged due to lateral spreading deformation.

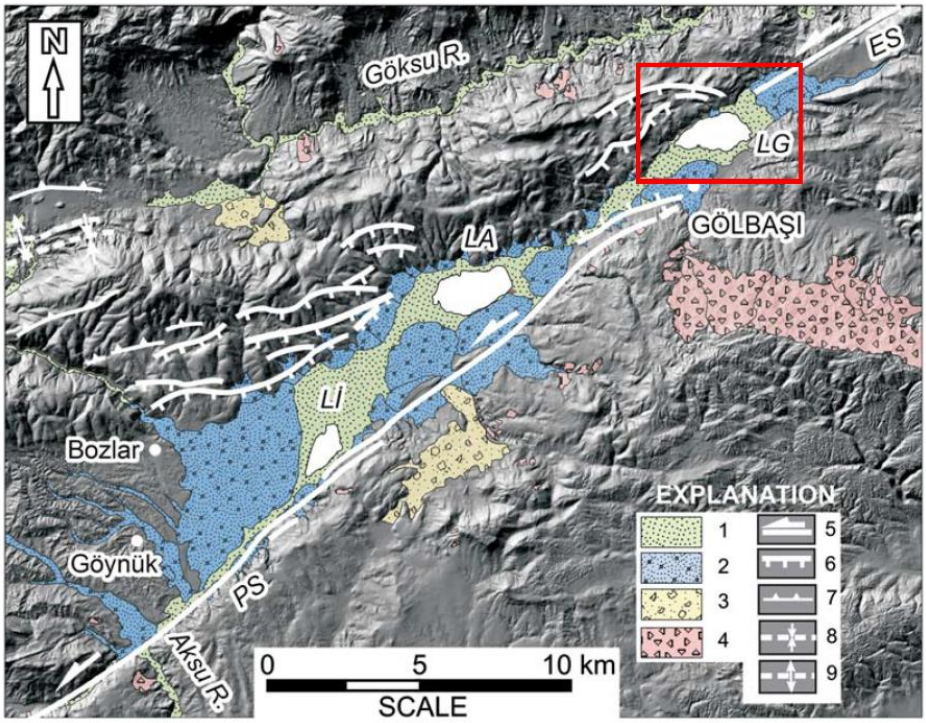


**Figure 14.** Active fault and Quaternary geological map of the Lake Gölbası releasing stepover and its vicinity, from Duman & Emre (2013). Inset box shows the location of previous Figure 13. ES, Erkenek segment; PS, Pazarcık segment; LG, Lake Gölbası; LI˙, Lake Inekli; LA, Lake Azaplı; R, river; (1) Holocene river bed and lake deposits; (2) Holocene fan deposits; (3) undifferentiated terrace deposits; (4) landslide deposits; (5) left-lateral strike-slip fault; (6) normal fault; (7) Southeastern Anatolian Thrust Zone; (8) syncline; (9) anticline.

In this last section, we present a number of different types of liquefaction phenomena identified in optical satellite imagery along the M7.7 earthquake rupture. Work in progress involves acquiring and examining new imagery over the affected areas, detailed mapping of the sites and of individual liquefaction features (Figure 18) and study of the paleogeography and fluvial settings in order to extract useful insights for future susceptibility studies (Taftsoglou et al. 2022).

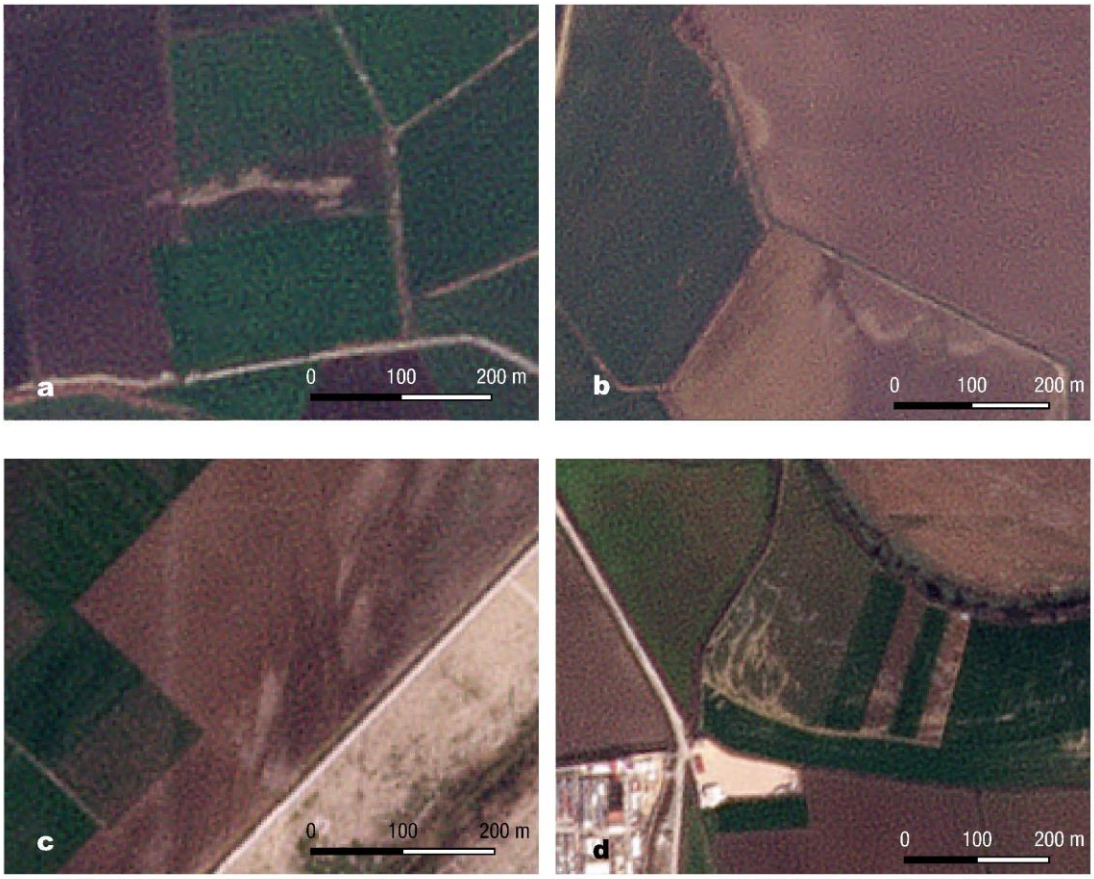


**Figure 15.** Examples of liquefaction phenomena mapped with Planet imagery; a) Liquefaction fissure (37.346N,36.869E), b) liquefaction ejecta (37.536N,36.875E), c) liquefaction ejecta along the surface ruptures west of Hatay airport (36.354N,36.272E), d) liquefaction fissures and sand boils (36.237N,36.3572E).

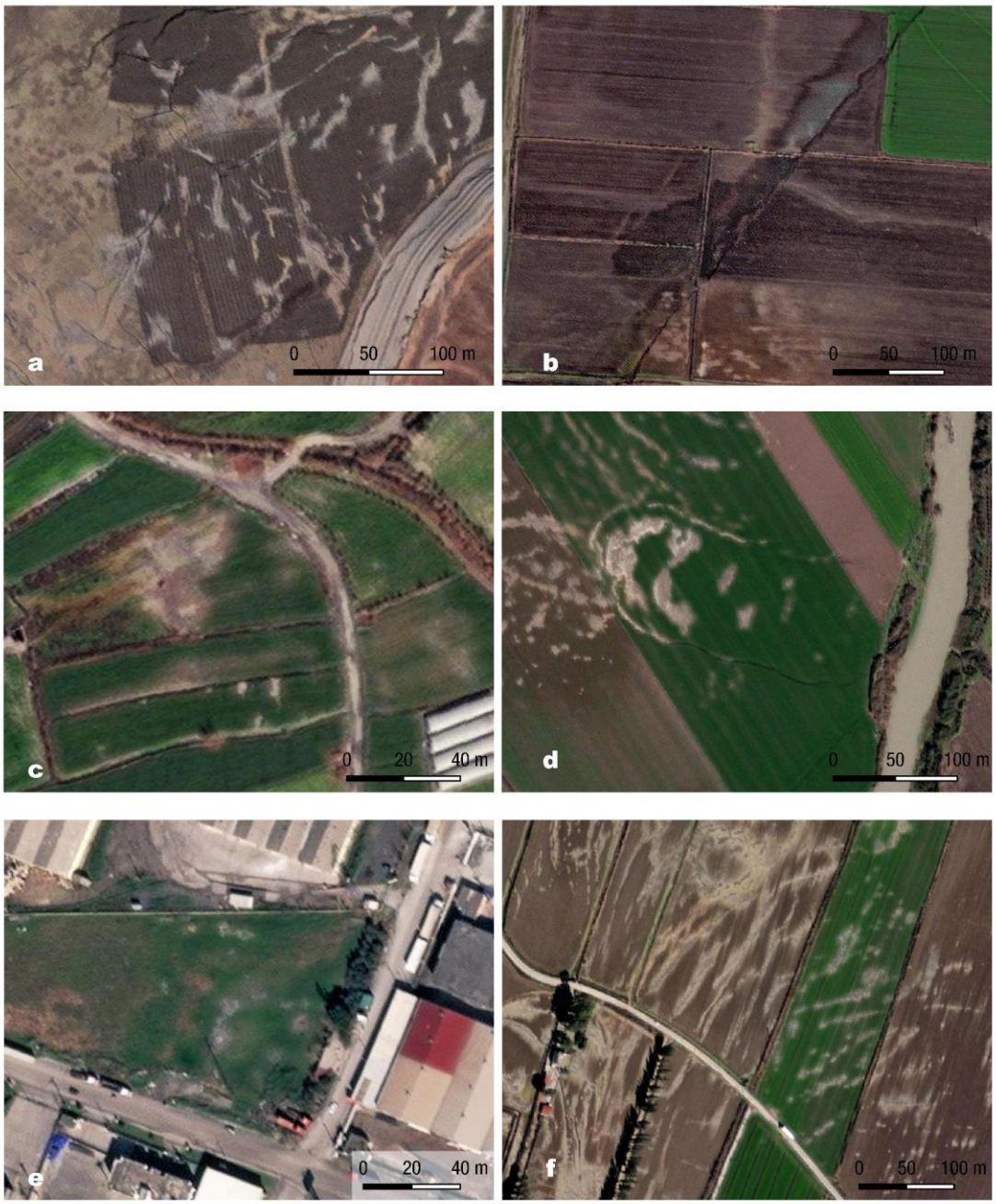


**Figure 16.** Examples of liquefaction phenomena mapped with very high resolution Maxar Open Data imagery; a) Liquefaction fissures and sand boils (37.50N,37.288E), b) liquefaction material ejected from surface fault rupture (37.404N,36.904E), c) sand boils and craters (36.048N,35.974E), d) liquefaction fissures, sand boils and lateral spreading along Asi (Orontes) river (36.252N,36.236E), e) liquefaction craters in Iskenderun, near the port (36.605N,36.201E), f) liquefaction fissures and sand boils (36.2566N,36.349E).

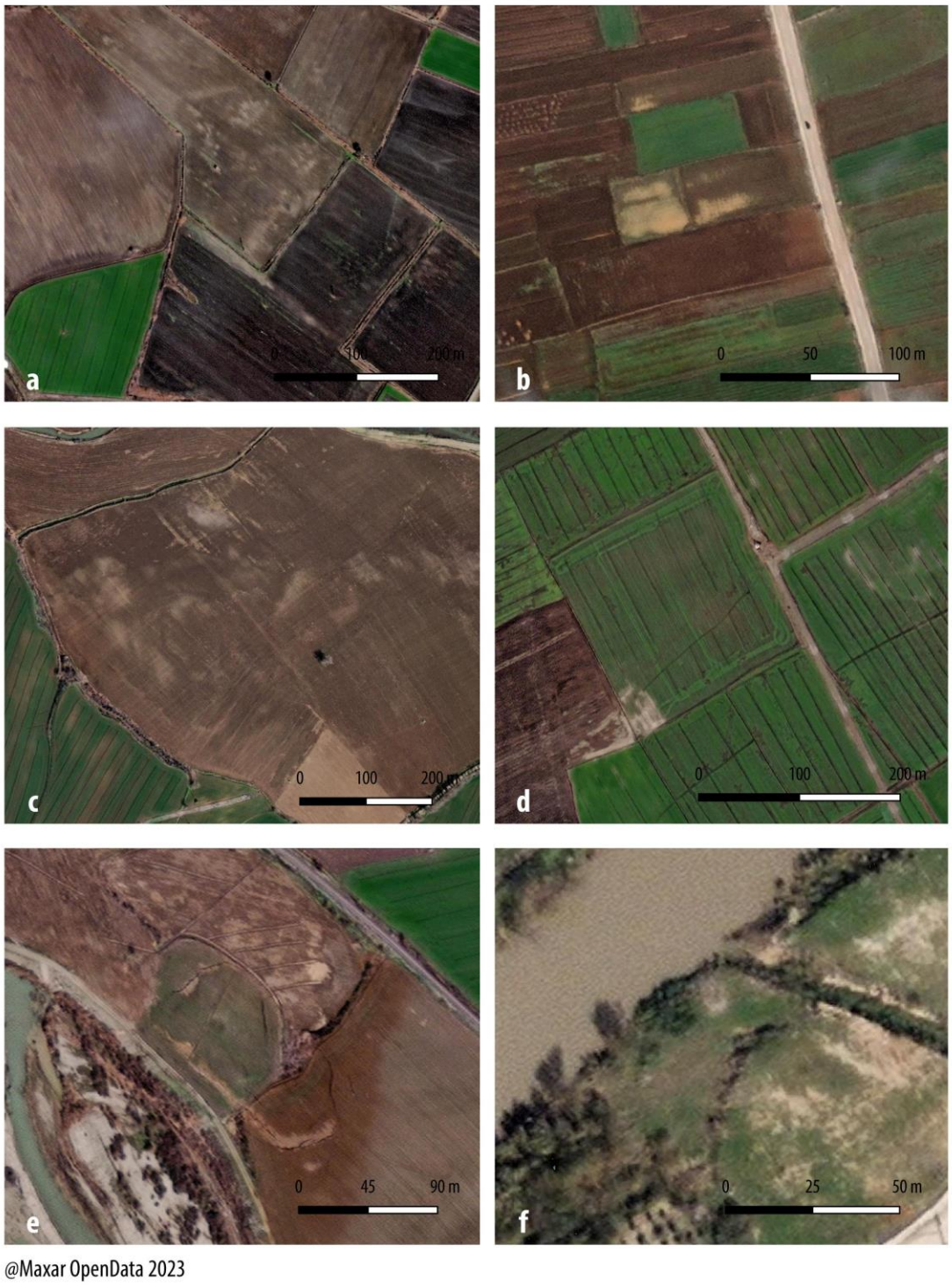


**Figure 17.** Examples of liquefaction phenomena mapped with very high resolution Maxar Open Data imagery; a) Liquefaction ejecta (37.391N,36.908E), b) liquefaction ejecta (35.988N,36.051E), c) sand boils and fissures (37.543N,36.869E), d) liquefaction ejecta (37.333N,36.868E), e) lateral spreading and sand fissures (37.407N,36.919E), f) lateral spreading along Asi (Orontes) river (36.065N,35.988E).

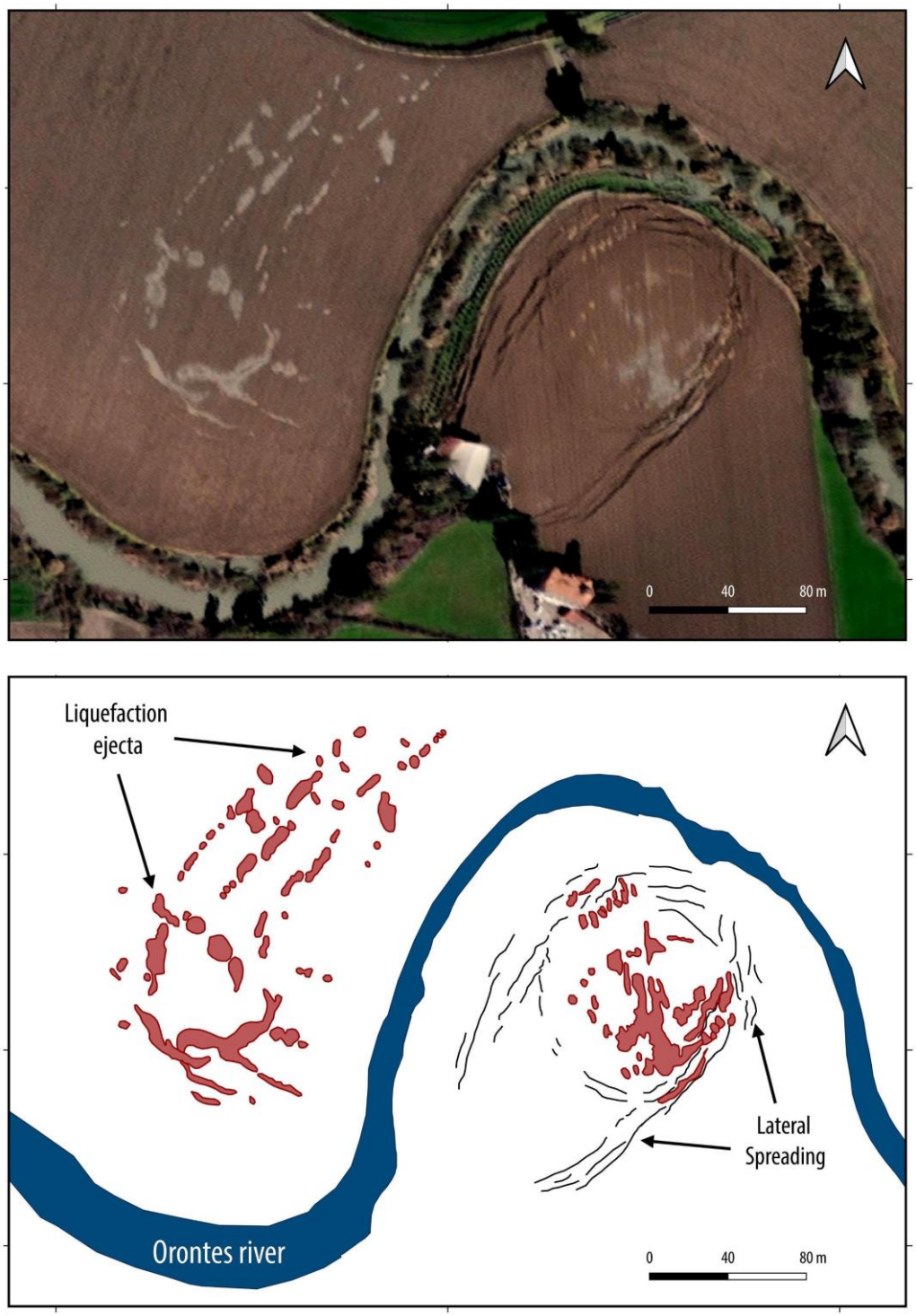


**Figure 18.** Work in progress; mapping liquefaction and lateral spreading features in detail. An example from Orontes (Asi) river, north-east of Antakya. VHR imagery from Maxar Open Data Program (above) and mapped individual features (below).

## 5. Acknowledgments – Data sources

Copernicus Sentinel-1 and Sentinel-2 imagery was accessed through Copernicus Open Access Hub (https://scihub.copernicus.eu/). Copernicus Global Digital Elevation Model, distributed by OpenTopography (https://doi.org/10.5069/G9028PQB). WorldView and GeoEye-1 imagery was accessed through Maxar's Open Data Program (https://www.maxar.com/open-data/turkey-earthquake-2023).

Planet Team (2023). Planet Application Program Interface: In Space for Life on Earth. San Francisco, CA. https://api.planet.com / Planet (Planet Labs, Inc., San Francisco, CA, USA)

## 6. References

Allen, C. R., 1969. Active faulting in northern Turkey. Rep. Div. of Geol. Sic., Calif. Inst. of Technol., Pasadena., 1577, 32 pp.

Ambraseys, N.N., 1988. Engineering seismology. Int. J. Earthq. Eng. Struct. Dyn. 17, 1–105

Ambraseys N. N. 2009. Earthquakes in the Mediterranean and Middle East: A multidisciplinary study of seismicity up to 1900. Cambridge University Press. 947pp. ISBN 978 0 521 87292 8.

Ambraseys N. N. and Finkel C. F. 1995. The seismicity of Turkey and adjacent areas: A historical review, 1500–1800. pp. 240.

Coskun, B. 1994. Oil possibilities of duplex structures in the Amik-Reyhanli basin, SE Turkey. Journal of Petroleum Geology, 174, 461-473

Duman, T., Emre, O. 2013. The East Anatolian Fault: geometry, segmentation and jog characteristics. In: Robertson, A. H. F., Parlak, O. & Unlugenc, U. C., (eds) Geological Development of Anatolia and the Easternmost Mediterranean Region. Geological Society, London, Special Publications, 372, http://dx.doi.org/10.1144/SP372.14

Guidoboni, E., Comastri, A. and Traina, G. 1994. Catalogue of Ancient Earthquakes in the Mediterranean Area up to the 10th Century. ING, Roma-SGA, Bologna.

Guidoboni E., Comastri A., 2005. Catalogue of earthquakes and tsunamis in the Mediterranean area from the 11th to the 15th century. INGV-SGA, Bologna, 1037 pp.

Hauksson, E., Olson, B., Grant, A., Andrews, J.R., Chung, A., Hough, S., Kanamori, H., McBride, S., Michael, A., Page, M., Ross, Z., Smith, D., Valkaniotis, S. 2020. The Normal-Faulting 2020 Mw 5.8 Lone Pine, Eastern California, Earthquake Sequence. Seismological Research Letters, https://doi.org/10.1785/0220200324

Hempton, M.R., 1985. Structure and deformation history of the Bitlis suture near Lake Hazar, southeastern Turkey. Geol. Soc. of America Bulletin, 96, 233–243.

Herece, E., 2008. ATLAS of East Anatolian Fault (EAF), General Directorate of Mineral Research and Exploration of Turkey (MTA), Special Publications, Serial Number 13, 359 pages with 13 sheets of Active Fault Segments Mapped in 1:100.000 scale, ISBN: 978-605-4075-12-6, December 5, 2008, Ankara, Turkey.

Karatas, A. 2014. Hydrographic Planning of Karasu Stream Basin (in Turkish). Unpublished Doctoral Thesis. İ.U. Sosyal Bilimler Enstitusu Cografya ABD, Istanbul.

Melgar, D., Ganas, A., Taymaz, T., Valkaniotis, S., Crowell, B., Kapetanidis, V., Tsironi, V., Yolsal-Çevikbilen, S., Öcalan, T. 2020. Rupture Kinematics of January 24, 2020 Mw 6.7 Doğanyol-Sivrice, Turkey Earthquake on the East Anatolian Fault Zone Imaged by Space Geodesy. Geophysical Journal International, ggaa345 https://doi.org/10.1093/gji/ggaa345

Melgar, D., Taymaz, T., Ganas, A., Crowell, B, Ocalan, T., Kahraman, M., Tsironi, V., Yolsal-Cevikbil, S., Valkaniotis, S., Irmak, T., Eken, T., Erman, C., Ozkan, B., Dogan, A.H., Altuntas, C., 2023. Sub-and super-shear ruptures during the 2023 Mw 7.8 and Mw 7.6 earthquake doublet in SE Türkiye. EarthArxiv, https://doi.org/10.31223/X52W9D

MTA, 2002. Geological map of Turkey (1:500.000 scale Adana and Hatay sheets). Ankara: General Directorate of Mineral Research and Exploration.

Papathanassiou, G., Pavlides, S., Christaras, B., Pitilakis, K., 2005. Liquefaction case histories and empirical relations of earthquake magnitude versus distance from the broader Aegean region. J Geodyn., 40(2–3), 257–78.

Papathanassiou, G., Ganas, A., Valkaniotis, S., 2016. Recurrent liquefaction-induced failures triggered by 2014 Cephalonia, Greece earthquakes: Spatial distribution and quantitative analysis of liquefaction potential. Engineering Geology, 200, 18-30. https://doi.org/10.1016/j.enggeo.2015.11.011

Papathanassiou, G., Valkaniotis, S., Ganas, A., Stampolidis, A., Rapti, D., Caputo, R. 2022. Floodplain evolution and its influence on liquefaction clustering: The case study of March 2021 Thessaly, Greece, seismic sequence. Engineering Geology, 298 (5), 106542 https://doi.org/10.1016/j.enggeo.2022.106542

Reilinger, R. et al., 2006. GPS constraints on continental deformation in the Africa–Arabia–Eurasia continental collision zone and implications for the dynamics of plate interactions, J. geophys. Res., 111, B05411, https://doi.org/10.1029/2005JB004051

Rojay, B., Heimann, A., Toprak, V., 2001. Neotectonic and volcanic characteristics of the Karasu fault zone (Anatolia, Turkey): the transition zone between the Dead Sea transform and the East Anatolian fault zone. Geodinamica Acta, 14, 197–212.

Şaroğlu, F., Emre, Ö., Kuşçu, İ., 1992a. The East Anatolian Fault Zone of Turkey, Special Issue, Annales Tectonicae 6, 99-125.

Şaroğlu, F., Emre, Ö., Kuşçu, İ., 1992b. Active Fault Map of Turkey, 2 sheets, General Directorate of Mineral Research and Exploration-MTA, Ankara, Turkey.

Taftsoglou, M., Valkaniotis, S., Papathanassiou, G., Klimis, N., Dokas, I. 2022. A Detailed Liquefaction Susceptibility Map of Nestos River Delta, Thrace, Greece Based on Surficial Geology and Geomorphology. Geosciences, 12 (10), 361 https://doi.org/10.3390/geosciences12100361

Tan, O., Taymaz, T. 2006. Active Tectonics of the Caucasus: Earthquake Source Mechanisms and Rupture Histories Obtained from Inversion of Teleseismic Body-Waveforms. In: Post-Collisional Tectonics and Magmatism in the Mediterranean Region and Asia, Geological Society of America, Special Paper 409, 531-578, https://doi.org/10.1130/2006.2409(25)

Taymaz, T., Eyidoğan, H., & Jackson, J.A. 1991a. Source Parameters of large earthquakes in the East Anatolian Fault Zone (Turkey). Geophysical Journal International, 106, 537-550, https://doi.org/10.1111/j.1365-246X.1991.tb06328.x

Taymaz, T., Ganas, A., Yolsal-Cevikbilen, S., Vera, F., Eken, T., Erman, C., Keles, D., Kapetanidis, V., Valkaniotis, S., Karasante, I., Tsironi, V., Gaebler, P., Melgar, D., Ocalan, T. 2021. Source Mechanism and Rupture Process of the 24 January 2020 Mw 6.7 Doğanyol–Sivrice Earthquake obtained from Seismological Waveform Analysis and Space Geodetic Observations on the East Anatolian Fault Zone (Turkey). Tectonophysics, https://doi.org/10.1016/j.tecto.2021.228745

Taymaz, T., Ganas, A., Berberian, M., Eken, T., Irmak, T.S., Kapetanidis, V., Yolsal-Çevikbilen, S., Erman, C., Keleş, D., Esmaeili, C., Tsironi, V., Özkan, B. 2022. The 23 February 2020 Qotur-Ravian Earthquake Doublet at the Iranian-Turkish Border: Seismological and InSAR Evidence for Escape Tectonics, Tectonophysics, Vol. 838, TECTO15364-229482, https://doi.org/10.1016/j.tecto.2022.229482

Tolun N., Pamir H.N. 1975. Hatay. 1:500 000 ölçekli Türkiye jeoloji haritasi, M.T.A. Ankara, 1975.

Trifonov, V.G. et al. 2018. Pliocene–Early Pleistocene history of the Euphrates valley applied to Late Cenozoic environment of the northern Arabian Plate and its surrounding, eastern Turkey, Quat. Int., 493, 137–165.

Yener, K., Edens, C., Harisson, T., Verstraete, J., Wilkinson, T.J. 2000. The Amuq Valley Regional Project, 1995-1998. American Journal of Archaeology, 104, No. 2, 163-220. https://doi.org/10.2307/507449

Yolsal-Çevikbilen, S., Taymaz, T., 2012. Earthquake source parameters 1325 along the Hellenic subduction zone and numerical simulations of historical tsunamis in the Eastern Mediterranean. Tectonophysics, 536–537, 61-100.

Yolsal-Çevikbilen, S., Taymaz, T., Helvaci, C., 2014. Earthquake mechanisms in the Gulfs of Gökova, Sığacık, Kuşadası and the Simav Region (western Turkey): neotectonics, seismotectonics and geodynamic implications. Tectonophysics, 635, 100-124.